The Canadian Mineralogist
Vol. 35, pp. 909-922 (1997)

EPITACTIC OVERGROWTHS AND INTERGROWTHS OF CLINOPYROXENE ON ORTHOPYROXENE: IMPLICATIONS FOR PATHS OF CRYSTALLIZATION, 1881 LAVA FLOW, MAUNA LOA VOLCANO, HAWAII

JAMES NICHOLLS[1] AND MAVIS Z. STOUT

Department of Geology and Geophysics, University of Calgary, Calgary, Alberta T2N 1N4

ABSTRACT

The 1881 tholeiite lava flow on Mauna Loa Volcano, Hawaii, contains epitactic overgrowths and intergrowths of clinopyroxene on orthopyroxene. The clinopyroxene overgrowths form only on faces parallel to the optic axial plane of orthopyroxene, (100). The lava flow contains microphenocrysts of olivine and pyroxene in a fine-grained groundmass of plagioclase, three pyroxenes, opaque minerals, and dark glass. The average composition of orthopyroxene is $En_{85\pm3}$. The epitactic overgrowths consist of clinopyroxene whose composition ranges from pigeonite to augite. The pyroxenes forming the epitactic overgrowths can be distinguished from one another by their relief against orthopyroxene in sections cut normal to (100). The olivine microphenocrysts are normally zoned, with a range in composition from Fo_{82} to Fo_{73}. Plagioclase is a groundmass phase in the 1881 lava flow and displays normal zoning. Crystallization paths predicted by thermodynamic modeling (MELTS) reproduce the mineral compositions found. The crystallization sequence required by the epitactic relationship is orthopyroxene followed by pigeonite or augite. The skeletal nature of the olivine is consistent with its saturation later than orthopyroxene. At pressures greater than 0.18 GPa, melts with the composition of the rock never become saturated with olivine. If, however, a fractionation path is followed at a pressure greater than 0.18 GPa, then the sequence of pyroxenes found in the epitactic overgrowths would be developed. If, after reaching clinopyroxene saturation, the magma is transported to shallower depths where pressures are less than approximately 0.1 GPa, then the melt would become saturated in olivine.

Keywords: tholeiite, basalt, epitactic growth, clinopyroxene, orthopyroxene, crystal fractionation, olivine, indices of refraction, extinction angles, birefringence, relief, Mauna Loa, Hawaii.

SOMMAIRE

La coulée de lave tholéiitique de 1881 provenant du volcan Mauna Loa, à Hawaii, contient des surcroissances et des intercroissances épitactiques de clinopyroxène sur orthopyroxène. Les surcroissances de clinopyroxène recouvrent seulement les faces parallèles au plan axial optique de l'orthopyroxène, (100). La coulée contient des microphénocristaux d'olivine et de pyroxène dans une pâte à granulométrie fine contenant plagioclase, trois pyroxènes, des minéraux opaques, et un verre foncé. La composition moyenne de l'orthopyroxène est $En_{85\pm3}$. Les surcroissances épitactiques sont faites de clinopyroxène dont la composition va de pigeonite à augite. Il est possible de distinguer les pyroxènes en croissance épitactique par leur relief par rapport à l'orthopyroxène dans des sections coupées perpendiculairement à (100). Les microphénocristaux d'olivine sont zonés normalement, et varient en composition de Fo_{82} à Fo_{73}. Le plagioclase dans cette coulée est limité à la pâte, et montre aussi une zonation normale. Les tracés de cristallisation prédits par le modèle thermodynamique MELTS reproduisent la composition des minéraux. La séquence de cristallisation imposée par la relation épitactique indique orthopyroxène suivi de pigeonite ou augite. La nature squelettique de l'olivine concorde avec sa saturation plus tard que l'orthopyroxène. A une pression supérieure à 0.18 GPa, un liquide ayant la composition de la roche ne deviendrait jamais saturé en olivine. Si, toutefois, le fractionnement se déroule à une pression supérieure à 0.18 GPa, la séquence des pyroxènes prédite selon les intercroissances épitactiques serait celle qui est observée. Si, une fois la saturation en clinopyroxène atteinte, le magma est transporté vers la surface, dans un milieu où la pression est inférieure à 0.1 GPa, il deviendrait saturé en olivine.

(Traduit par la Rédaction)

Mots-clés: tholéiite, basalte, croissance épitactique, clinopyroxène, orthopyroxène, fractionnement de cristaux, olivine, indices de réfraction, angles d'extinction, biréfringence, relief, Mauna Loa, Hawaii.

[1] *E-mail address*: nicholls@geo.ucalgary.ca

INTRODUCTION

Several samples of Mauna Loa tholeiites contain overgrowths and intergrowths of clinopyroxene on orthopyroxene. For example, some flows from the 1880, 1887, 1926 (Basaltic Volcanism Study Project 1981), and 1943 sequences of eruptions display such textures. A sketch of one overgrown crystal of orthopyroxene from a flow that erupted in 1881 as one in a sequence of eruptions that began in 1880 is shown on Figure 1A. The clinopyroxene overgrowths form only on faces parallel to the optic axial plane of orthopyroxene. Two optical orientations for orthopyroxene are quoted in the literature. Deer *et al.* (1992) set the optic axial plane of orthopyroxene parallel to (100), whereas Phillips & Griffen (1981) set it parallel to (010). All orthopyroxenes have the same optical orientation. Consequently, the different descriptions result from different choices for the axis of the unit cell of orthopyroxene. The orientation described by Deer *et al.* (1992) is the better choice because the *b* and *c* axes of the two pyroxenes, clinopyroxene and orthopyroxene, are approximately the same length, and the atomic arrangements in the (100) plane are similar; both factors promote epitactic growth. In sections where the orthopyroxene shows intersecting cleavages, so do the clinopyroxene overgrowths (Fig. 2A). Hence, the *c* axes of the two minerals are parallel. The relation between the optical orientations is shown in Figure 1B. The epitactic overgrowths have the same orientations as exsolution lamellae of augite in orthopyroxene (Hess 1960). Epitactic minerals are exact forms of reaction fabrics (Lauder 1961) in which the orientation of one mineral influences the orientation of another mineral during crystallization. Tarney (1969) described epitactic overgrowths of augite on orthopyroxene from dikes near Lochinver, Scotland, as well as the reverse, orthopyroxene on augite. In this paper, we describe overgrowths of both Ca-rich and Ca-poor clinopyroxene on orthopyroxene, and the optical properties that distinguish the two clinopyroxenes in an epitactic relationship.

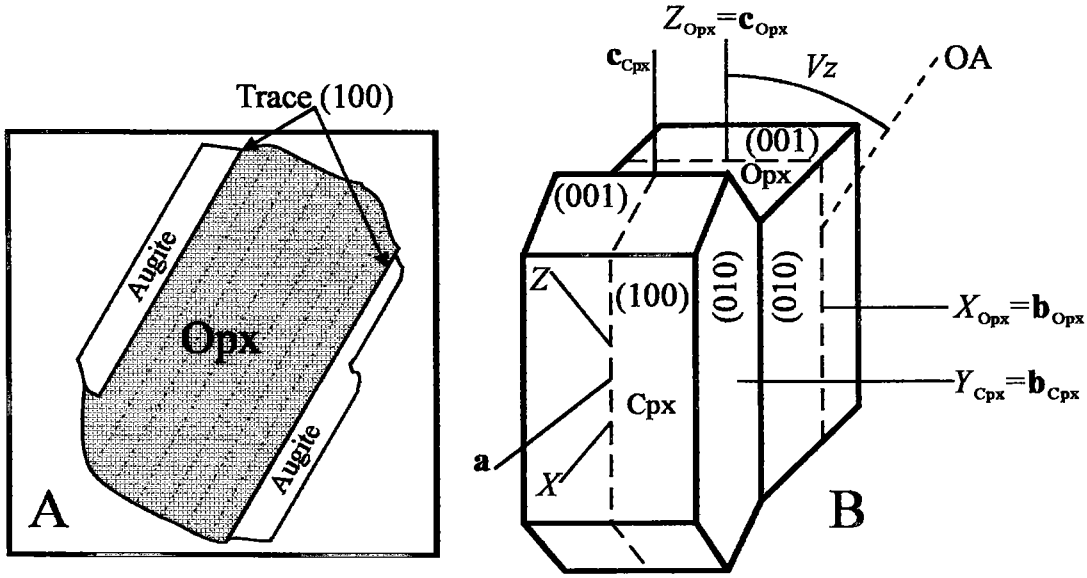

FIG. 1. A. Sketch of clinopyroxene overgrowth on orthopyroxene from the 1881 Mauna Loa tholeiite basalt. B. Orientation of orthopyroxene and augite crystals in position of epitactic growth. The (100) faces of the two crystals coincide. OA: optic axis.

SAMPLE DESCRIPTION

The sample described in this paper was collected from the lower slopes of Mauna Loa Volcano, Hawaii, on the outskirts of Hilo. The flow erupted from the northeast rift zone of Mauna Loa at an elevation below 3660 m (Lockwood & Lipman 1987) and flowed northeastward, down the northeastern slope of the volcano.

The light gray rock contains microphenocrysts of olivine and pyroxene in a fine-grained groundmass. The olivine microphenocrysts are nearly equant, commonly skeletal, and enclose groundmass assemblages. The microphenocrysts of epitactic pyroxene range between 200×125 μm and 550×200 μm. Orthopyroxene forms the core of the microphenocrysts and is commonly bounded by crystal faces, whereas the clinopyroxene has grown onto the (100) faces of the orthopyroxene and usually has an irregular outer surface. In some cases, the core of the microphenocrysts contains tabular inclusions of clinopyroxene with planar boundaries. The tabular inclusions

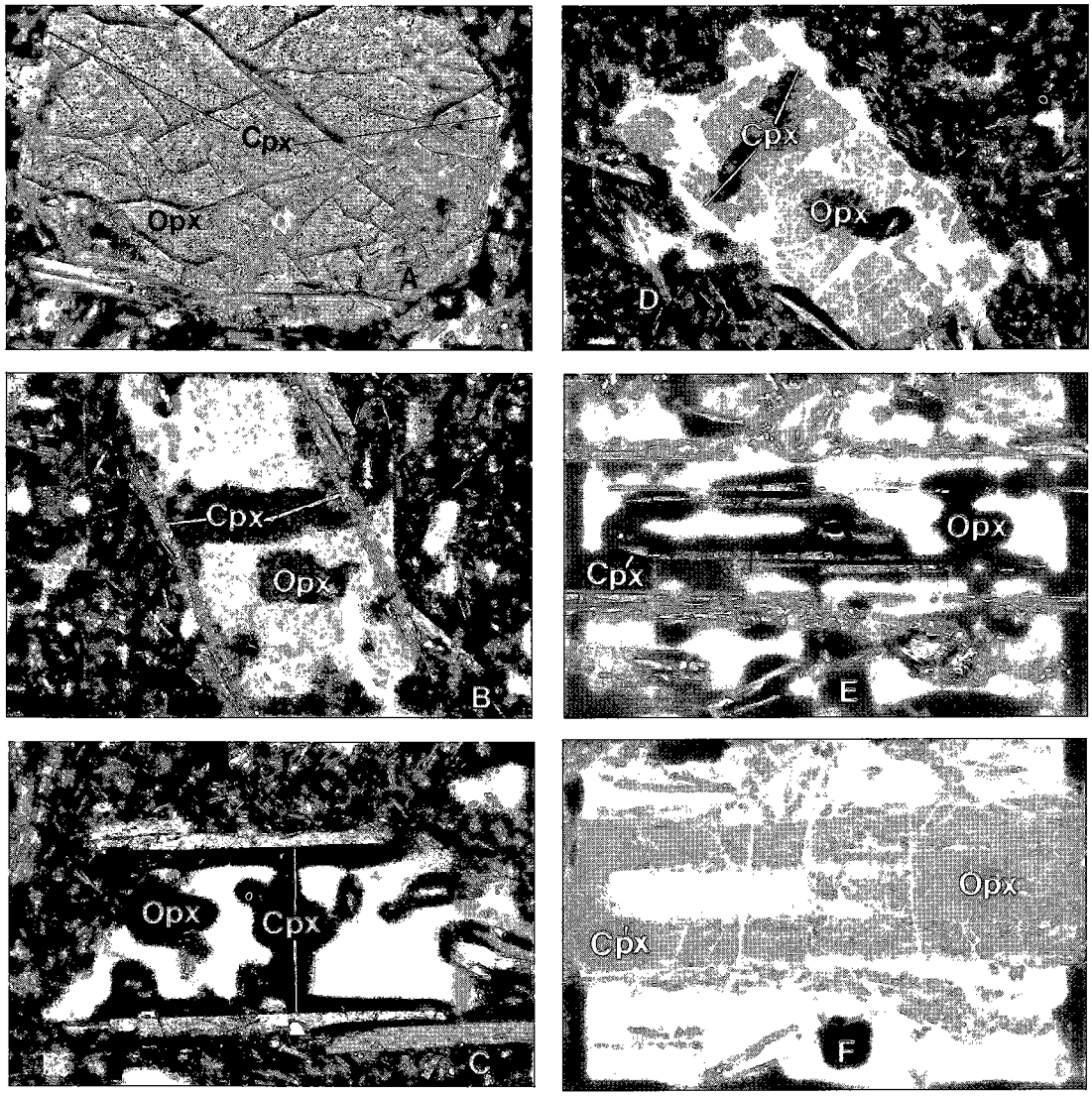

FIG. 2. A. Section cut normal to the *c* axis of orthopyroxene with epitactic overgrowth of clinopyroxene on (100). Cleavage is continuous across the contact surface. Plane-polarized light. B. Orthopyroxene with epitactic overgrowth of augite on (100). Crossed polars. Section cut normal to (100) and close to an optic axis in orthopyroxene. C. Orthopyroxene at extinction. Section cut normal to (100). Crossed polars. D. Same crystal as C. Section rotated to the extinction position of clinopyroxene overgrowth. Crossed polars. E. Orthopyroxene with clinopyroxene overgrowths and intergrowths. Intergrowths are tabular with large surfaces parallel to (100). Crossed polars. F. Same crystal as E. Uncrossed polars. Note the low relief between pigeonite intergrowth and orthopyroxene.

have their extensive surfaces parallel to the (100) faces of the host orthopyroxene (Fig. 2). The intergranular groundmass, consisting of plagioclase, three pyroxenes, opaque minerals, and dark glass, contains clusters of microlites of the same phases.

A mode of a sample from the 1881 lava flow is listed in Table 1. The mode was determined by identifying spots with the electron microprobe (Nicholls & Stout 1986). Constituents in much of the groundmass cannot be identified because of their small grain-size, especially in the clusters of microlites. Unidentified spots make up 32% of the total (Table 1). The modal amounts of the various pyroxenes listed in Table 1 were estimated from intensity ratios of Ca radiation, in addition to ranking the intensities of peaks

TABLE 1. MODE AND COMPOSITION OF THE 1881 THOLEIITIC BASALT

Olivine	2.96	(0.36)	SiO_2	51.85
Orthopyroxene (0 - 3% CaO)	2.68	(0.33)	TiO_2	1.93
Pigeonite (4 - 10% CaO)	5.73	(0.79)	Al_2O_3	14.04
Subcalcic Augite (11 - 15% CaO)	22.50	(0.90)	Fe_2O_3	1.56
Augite (16 - 21% CaO)	8.03		FeO	9.16
Plagioclase	51.51	(1.07)	MnO	0.17
Fe-Ti Oxides	6.35	(0.51)	MgO	7.85
Fe-rich opaque mineral (sulfide)	0.24	(0.10)	CaO	10.45
			Na_2O	2.07
			K_2O	0.37
			P_2O_5	0.22

Mode: total number of spots: 4779; vesicles: 1700; spots identified: 2093, 68%. Glass included in unidentified spots. Standard deviations of the modal values, shown in parentheses, are based on a binomial distribution of the probability of a phase being present or absent at a location on the thin section. Standard deviation for subcalcic augite includes that for augite. Rock composition from Macdonald & Katsura (1964, anal. 6, p. 123). The proportion of oxides is quoted in wt.%.

from eight elements (Nicholls & Stout 1986). Consequently, the sum of the concentrations of the pyroxenes has the same precision and accuracy as the concentrations of the other phases, but the concentrations of the individual kinds of pyroxenes are more approximate [see Nicholls & Stout (1986) for a discussion of the precision and accuracy of modal analyses with the electron microprobe].

MINERALOGY

Pyroxene compositions

The 1881 lava flow contains three pyroxenes: orthopyroxene (enstatite), Ca-poor clinopyroxene (pigeonite and subcalcic augite, Fig. 3A), and Ca-rich clinopyroxene

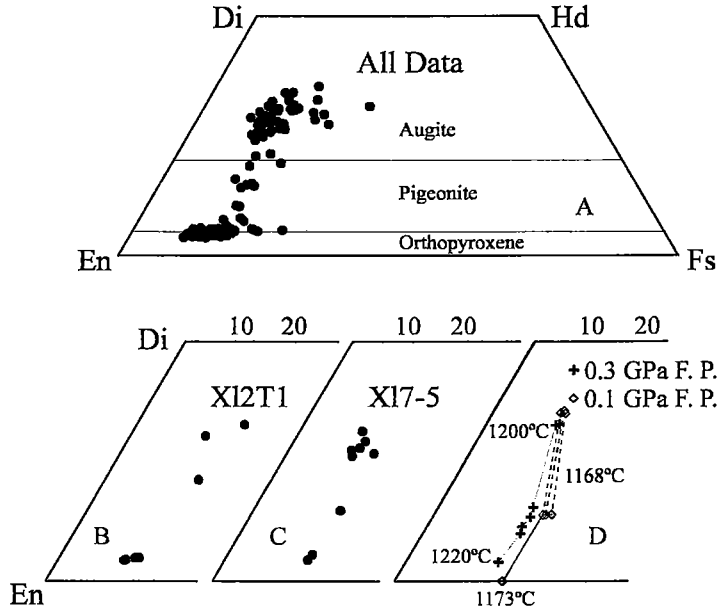

FIG. 3. Closed circles represent the composition of the pyroxene grains. A. Compositions of pyroxenes in epitactic orientations from the 1881 lava flow from Mauna Loa. Pyroxene names from Morimoto (1989). B and C. Compositions of phases in epitactic growth from single grains. D. Predicted compositions of pyroxenes produced by fractional crystallization of a melt that has an initial composition equal to the rock composition listed in Macdonald & Katsura (1964, Table 8, anal. 6, p. 123). Compositions calculated with thermodynamic data compiled by Ghiorso & Sack (1995). F.P.: fractionation path. Dashed lines connect compositions of coexisting pyroxenes in the thermodynamic model. Composition at 1173°C shows the Fe:Mg ratio of the olivine on the liquidus.

TABLE 2. RESULTS OF ELECTRON-MICROPROBE ANALYSES AND MINERAL FORMULAE OF PYROXENES IN EPITACTIC GROWTHS

	xl2t1e1	xl2t1e1	xl2t1r1	xl2t1m1	xl2t1c1	xl2t1m2	xl2t1r2	xl2t1e2
SiO_2	53.59	50.80	53.49	52.79	53.15	52.83	52.88	50.02
TiO_2	0.69	1.02	0.36	0.38	0.36	0.35	0.38	1.44
Al_2O_3	2.23	3.52	1.67	2.15	2.04_3	2.13	1.54	2.69
FeO	12.72	11.37	11.48	11.09	11.15	11.07	12.03	15.08
MnO	0.26	0.24	0.25	0.22	0.21	0.21	0.24	0.26
MgO	21.71	18.18	28.77	29.40	29.53	29.31	28.64	15.16
CaO	10.93	15.12	2.57	2.29	2.35	2.34	2.55	15.98
Na_2O	0.11	0.18	0.00	0.00	0.00	0.00	0.00	0.19
Total	102.24	100.43	98.59	98.32	98.79l	98.24	98.26	100.82
			Number of ions on the basis of 12 positive charges					
Si	1.923	1.875	1.934	1.912	1.916	1.914	1.926	1.879
^{IV}Al	0.077	0.125	0.066	0.088	0.084	0.086	0.074	0.121
Total	2.000	2.000	2.000	2.000	2.000	2.000	2.000	2.000
Ti	0.019	0.028	0.010	0.010	0.010	0.010	0.010	0.041
Al	0.017	0.028	0.005	0.003	0.002	0.005	-0.008	-0.002
Fe^{2+}	0.382	0.351	0.347	0.336	0.336	0.335	0.366	0.474
Mn	0.008	0.008	0.008	0.007	0.006	0.006	0.007	0.008
Mg	1.161	1.000	1.551	1.587	1.586	1.583	1.555	0.849
Ca	0.420	0.598	0.100	0.089	0.091	0.091	0.100	0.643
Na	0.008	0.013	0.000	0.000	0.000	0.000	0.000	0.014
Total	2.015	2.026	2.021	2.032	2.031	2.030	2.030	2.027

	xl7-5e1	xl7-5e1	xl7-5e1	xl7-5r1	xl7-5c1	xl7-5r2	xl7-5r2	xl7-5r2	xl7-5e2
SiO_2	52.10	51.06	52.18	54.84	52.82	52.87	55.51	54.13	52.15
TiO_2	0.60	0.84	0.58	0.30	0.54	0.58	0.28	0.37	0.53
Al_2O_3	2.08	2.73	2.22	1.28	2.14	1.93	1.23	1.19	2.00
FeO	10.86	10.00	9.95	11.90	9.42	9.48	10.70	11.84	10.84
MnO	0.22	0.20	0.22	0.25	0.24	0.23	0.21	0.28	0.23
MgO	19.62	18.82	20.68	28.80	20.47	19.96	29.81	24.81	20.86
CaO	13.18	15.56	13.68	2.94	13.95	14.64	2.38	7.56	13.13
Na_2O	0.13	0.16	0.17	0.03	0.16	0.15	0.00	0.09	0.14
Total	98.79	99.37	99.68	100.34	99.74	99.84	100.12	100.27	99.88
				Number of ions on the basis of 12 positive charges					
Si	1.935	1.896	1.917	1.951	1.933	1.937	1.962	1.954	1.917
^{IV}Al	0.065	0.104	0.083	0.049	0.067	0.063	0.038	0.046	0.083
Total	2.000	2.000	2.000	2.000	2.000	2.000	2.000	2.000	2.000
Ti	0.017	0.023	0.016	0.008	0.015	0.016	0.007	0.010	0.015
Al	0.026	0.015	0.013	0.005	0.026	0.021	0.014	0.004	0.004
Fe^{2+}	0.337	0.310	0.306	0.354	0.288	0.291	0.316	0.357	0.333
Mn	0.007	0.006	0.007	0.008	0.007	0.007	0.006	0.009	0.007
Mg	1.086	1.041	1.132	1.527	1.117	1.090	1.571	1.335	1.143
Ca	0.525	0.619	0.538	0.112	0.547	0.575	0.090	0.292	0.517
Na	0.009	0.012	0.012	0.002	0.011	0.011	0.000	0.006	0.010
Total	2.007	2.026	2.024	2.016	2.011	2.011	2.004	2.013	2.029

The analytical results are quoted in wt.% oxides. Detection limit: 0.022 wt.% Na_2O; xl: crystal number; t: traverse number; e: epitactic overgrowth (Cpx); c, m, r: core, middle, rim. Spot compositions are presented in the order collected in each traverse across sample.

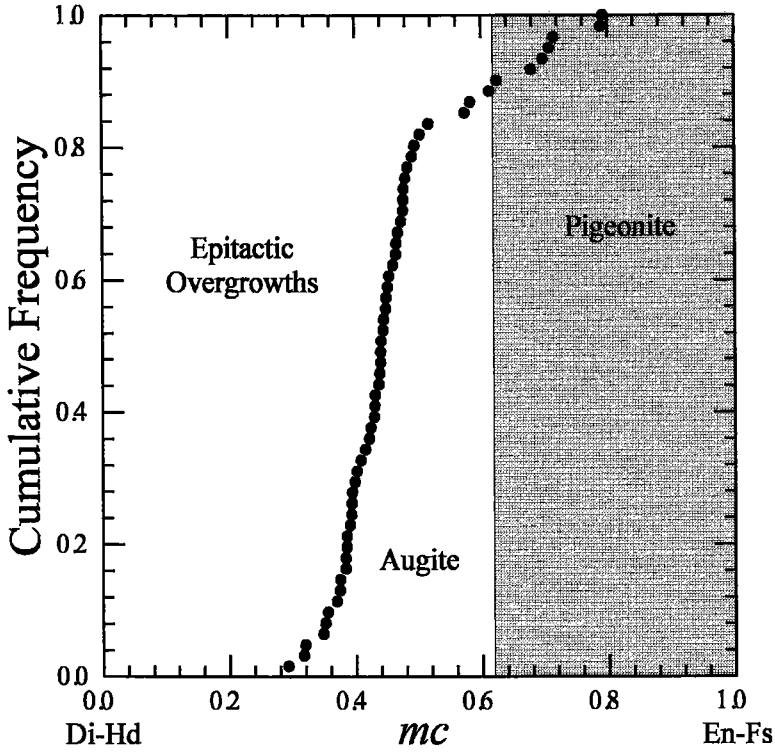

FIG. 4. Frequency distribution of compositions of epitactic overgrowths of clinopyroxenes on orthopyroxene. Shaded area separates pigeonite (Morimoto 1989) compositions from augite compositions. *mc* is the Thompson space variable (Thompson 1982) that represents the extent of Mg-for-Ca substitution in pyroxenes, $MgCa_{-1}$.

(augite) according to the IMA classification (Morimoto 1989). Results of electron-microprobe analyses of representative crystals with epitactic overgrowths are listed in Table 2 and illustrated in Figure 3A. The dominant part of each grain is orthopyroxene. Analyses of orthopyroxene were made at the center of a grain in thin section (c), approximately halfway between the center and the edge in the case of an overgrowth (m), and at the edge of the orthopyroxene grain, next to the overgrowth (r). Any single grain of orthopyroxene with epitactic overgrowths of clinopyroxene is almost unzoned (Figs. 3B, C), although there exists a range of compositions among several crystals (Fig. 3A). The range of core compositions is En_{88} to En_{77}, whereas the rim of the orthopyroxene crystals range from En_{89} to En_{73}. The average of all the core compositions is $En_{85\pm3}$. The same average and range were obtained for rim compositions.

The epitactic overgrowths are clinopyroxenes with a range of compositions from pigeonite to augite (Fig. 3A). Approximately 90% of the analyzed overgrowths are augite (Fig. 4); only 10% are identified as pigeonite. A table listing results of 165 electron-microprobe analyses of spots on pyroxene crystals with epitactic overgrowths is available from the Depository of Unpublished Data, CISTI, National Research Council of Canada, Ottawa, Ontario K1A 0S2.

Optical properties of epitactic pyroxenes

The Ca-poor and Ca-rich pyroxenes are difficult to distinguish in epitactic overgrowths. In addition, the initial overgrowth may be too thin to analyze with the electron microprobe. Consequently, careful optical examination is required to identify and determine the sequence of clinopyroxene overgrowth. This section presents a review of the optical properties of pyroxenes in sections cut normal to (100) and provides guidelines for distinguishing the clinopyroxenes in epitactic overgrowths.

Mineralogists and crystallographers have measured the principal indices of refraction, optic sign and optic axial angle ($2V$) of minerals for over a century. Unfortunately, different properties were measured by different investigators on different crystal fragments. The

TABLE 3. CONSISTENT VALUES OF $2V_z$ AND OF INDICES OF REFRACTION FOR ORTHOPYROXENE

fm	$2V_z$	α	β	γ
0.00	55.0	1.6494	1.6513	1.6586
0.20	79.8	1.6613	1.6655	1.6716
0.40	99.2	1.6733	1.6798	1.6845
0.60	113.0	1.6853	1.6937	1.6974
0.80	121.2	1.6972	1.7072	1.7103
1.00	124.0	1.7092	1.7201	1.7233
1.20	121.2	1.7212	1.7326	1.7362
1.40	113.0	1.7331	1.7442	1.7491
1.60	99.2	1.7451	1.7549	1.7621
1.80	79.8	1.7571	1.7644	1.7750
2.00	55.0	1.7691	1.7730	1.7879

Values of α and γ calculated from: $\alpha = 1.6494 + 0.05895\ fm$ and $\gamma = 1.6586 + 0.06465\ fm$. Values of β were calculated from values of α, γ and $2V_z$. The least-squares representation of the values of β is: $\beta = 1.6505 + 0.07774\ fm - 8.0535 \times 10^{-3}\ fm^2$. Optical orientation: $X = b$, $Y = -a$, $Z = c$.

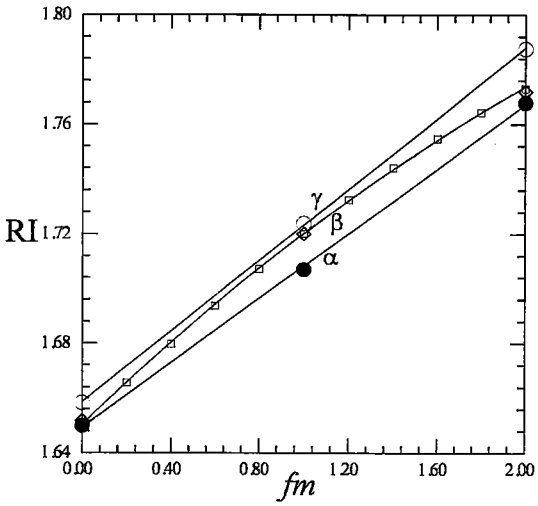

FIG. 5. Indices of refraction (RI) of orthopyroxene (Table 3).

optical properties are not all independent, and data in the literature commonly are internally inconsistent. In order to distinguish the different clinopyroxenes, optical data should first be tested for consistency and, if inconsistent, rendered consistent.

A method for obtaining internally consistent values for 2V and indices of refraction

The principal indices of refraction and *2V* are not independent properties because they are related by the equation (Wright 1951, Bloss 1961, p. 156):

TABLE 4. COMPOSITIONAL DEPENDENCE OF INDICES OF REFRACTION OF Ca-POOR CLINOPYROXENE WITH OAP NORMAL TO (010)

$\alpha = 1.6254 + 0.0308\ fm + 0.0658\ mc$	±0.0045
$\beta = 1.6288 + 0.0294\ fm + 0.0639\ mc$	±0.0045
$\gamma = 1.6655 + 0.0423\ fm + 0.0368\ mc$	±0.0054

$Z \wedge c = -49°$.

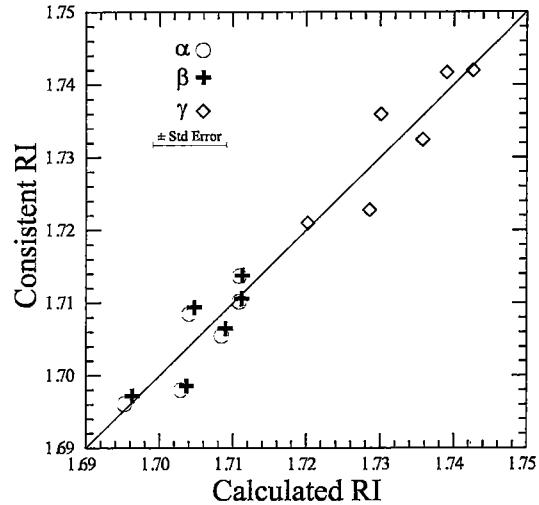

FIG. 6. Calculated and consistent values of indices of refraction for Ca-poor clinopyroxene with optic axial plane normal to (010) (Table 4).

$$\cos^2 V_z = [\alpha^2(\gamma^2 - \beta^2)]/[\beta^2(\gamma^2 - \alpha^2)] \quad (1)$$

Because of experimental errors, tabulated values of *2V* and the principal indices of refraction seldom exactly satisfy Equation (1). In some cases, calculated and measured values of *2V* differ by several degrees. The quality of determinative charts for minerals, in this case clinopyroxenes, depends on the consistency of the tabulated optical data used to construct them.

A method for calculating values of *2V* and indices of refraction that are consistent with Equation (1), and as close to the tabulated values as possible, makes use of Lagrange multipliers, and provides consistent data. This technique of constrained minimization is explained in many mathematics texts (*e.g.*, Thomas 1968, p. 528; Kaplan 1973, p. 184; Marsden & Tromba 1981, p. 217).

Consistency is a necessary requirement for accurate data, but it is not a sufficient one. If data are inconsistent, some or all of them are not correct. However, consistent data also may be inaccurate.

The mathematical procedure finds recalculated values for the optical properties such that the sum of squares of the differences between measured and recalculated values is a minimum, and also that the recalculated values satisfy equation (1). From measured principal indices of refraction, α, β, and γ, $2V_z$ can be calculated with Equation (1). The angle $2V$ can be measured as well and compared to the calculated value. It would be fortuitous if the two values agreed exactly, because of experimental error in determining both the indices of refraction and $2V$. The mathematical procedure leads to values of α, β, γ, and $2V$ such that the following function is a minimum:

$$F = (\alpha - \alpha')^2 + (\beta - \beta')^2 + (\gamma - \gamma')^2 + (2V_z - 2V_z')^2 + \vartheta\,[\alpha^2(\gamma^2 - \beta^2) - 0.5\,\beta^2(\gamma^2 - \alpha^2)\,(1 + \cos 2V_z)] \quad (2)$$

where the primes indicate measured or tabulated values, and ϑ is the Lagrange multiplier. The term in square brackets follows from Equation (1) by using a double-angle trigonometric formula. Equation (1) is the constraint on the minimization. Carrying through the mathematical procedure provides the following set of equations:

$$\alpha\,\{1 + \vartheta\,[\gamma^2 - \beta^2 + 0.5\,\beta^2(1 + \cos 2V_z)]\} - \alpha' = 0 \quad (3)$$

$$\beta\,\{1 - \vartheta\,[\alpha^2 + 0.5(\gamma^2 - \alpha^2)(1 + \cos 2V_z)]\} - \beta' = 0 \quad (4)$$

$$\gamma\,\{1 - \vartheta\,[\alpha^2 - 0.5\,\beta^2(1 + \cos 2V_z)]\} - \gamma' = 0 \quad (5)$$

$$2V_z + 0.25\,\vartheta\,\beta^2(\gamma^2 - \alpha^2)\sin 2V_z - 2V_z' = 0 \quad (6)$$

$$\alpha^2(\gamma^2 - \beta^2) - 0.5\,\beta^2(\gamma^2 - \alpha^2)(1 + \cos 2V_z) = 0 \quad (7)$$

Equations (3) through (7) are a set of five equations in five unknowns, α, β, γ, $2V_z$ and ϑ, that can be solved simultaneously. Unfortunately, the equations are nonlinear (*i.e.*, squares, higher powers, and trigonometric functions of the unknowns are present in the expressions), and their solution requires iteration techniques. Consequently, they are solved with a computer program. Burden *et al.* (1981, Chapter 9) and Press *et al.* (1992, Chapter 9) described methods for solving nonlinear systems of equations. The important point is that in theory and practice, consistent values of the optical parameters are produced.

Optical properties of orthopyroxene

Indices of refraction of orthopyroxene as a function of the Thompson space Fe-for-Mg substitution, *fm* or $FeMg_{-1}$ (Thompson 1982), are listed in Table 3 and displayed on Figure 5. Following Deer *et al.* (1978), α and γ are taken to vary linearly with *fm*. β was constrained to fit a second degree polynomial such that $2V_z$ is symmetrical and parabolic between the Fe and Mg end-members (Deer *et al.* 1978, p. 109).

Optical properties of Ca-poor clinopyroxene

Equations representing the compositional dependence of the indices of refraction of Ca-poor clinopyroxene with optical axial planes normal to (010) are listed in Table 4. The optical constants of six samples of pigeonite with complete optical data (Deer *et al.* 1978, Table 13) were first recalculated to consistent values and then fit to a linear model with two independent variables, *fm* and *mc*, where *mc* represents the Thompson space Mg-for-Ca substitution, $MgCa_{-1}$ (Thompson 1982). The quality of the fit can be judged by the information displayed in Figure 6. The optical properties of clinopyroxenes depend on both composition and degree of order of atoms in the structure. Consequently, the simple model in Table 4 cannot adequately represent all pyroxenes with optic axial planes normal to (010). However, for compositions near those of the six samples of pigeonite, the equations may be an adequate approximation. The *fm* values of the six samples range from 0.6245 to 1.1691, compared to more magnesian values between 0.1890 and 0.5866 in the Ca-poor pyroxene from the 1881 flow (Figs. 3, 4). The *mc* values of the six samples range from 0.7512 to 0.8197 and partly overlap the range from 0.69 to 0.79 in pigeonite from the 1881 flow. It follows that the indices of refraction for pigeonite in the 1881 flow are expected to differ from those for the six reference samples, mostly because of different *fm* values. The variation of β with composition depends mostly on *fm* at constant values for *mc* (see Deer *et al.* 1992, p. 183, Fig. 73). Presumably, the other indices of refraction do also. The difference in *fm* between the most magnesian pyroxene from the literature (0.6245) and the most magnesian pigeonite in the 1881 lava flow (0.1890) corresponds to an extrapolation at constant *mc* of less than three standard errors in index of refraction (Table 4); this value is not likely to lead to large errors, given the expected linear dependence of index of refraction on *fm*.

TABLE 5. TABULATED AND CONSISTENT OPTICAL PROPERTIES OF CLINOPYROXENE END-MEMBERS AND TWO SAMPLES OF AUGITE

	$2V_z$ (O)	$2V_z$ (C)	α (O)	α (C)	β (O)	β (C)	γ (O)	γ (C)	Z^c
Di	59.3	59.3021	1.664	1.6641	1.672	1.6713	1.694	1.6942	38.0
Hd	64	63.9944	1.730	1.7298	1.734	1.7363	1.754	1.7534	48.0
CEn	53.5	53.5005	1.651	1.6505	1.653	1.6524	1.660	1.6601	22.0
CFs	23	23.0021	1.764	1.7642	1.767	1.7653	1.792	1.7921	31.0
Ct	59	58.9980	1.7095	1.7094	1.714	1.7149	1.7325	1.7323	
Jd	60	60.0023	1.640	1.6401	1.645	1.6431	1.652	1.6525	40.0
Ae	119	118.9962	1.776	1.7760	1.819	1.8196	1.836	1.8355	100.0
Jh	70	69.9988	1.710	1.7100	1.719	1.7191	1.738	1.7388	48.0
S5	47	47.021	1.700	1.7001	1.705	1.7040	1.725	1.7252	46.0
S8	52	52.0023	1.710	1.7101	1.716	1.7150	1.736	1.7362	45.0

(O): original value, (C) consistent value. Symbols: Di diopside, Hd hedenbergite, CEn clinoenstatite, CFs clinoferrosilite, Ct Ca-Tschermaks pyroxene, Jd jadeite, Ae aegirine, Jh johannsenite. Samples of augite: S5: Deer *et al.* (1978, Table 31, number 5); S8: Deer *et al.* (1978, Table 33, number 8). Observed data taken from values compiled by Deer *et al.* (1978).

Optical properties of Ca-rich clinopyroxene

Consistent and observed optical properties for clinopyroxene end-members and two samples of augite are listed in Table 5. The differences between the observed and calculated properties are small, especially the values of $2V_z$.

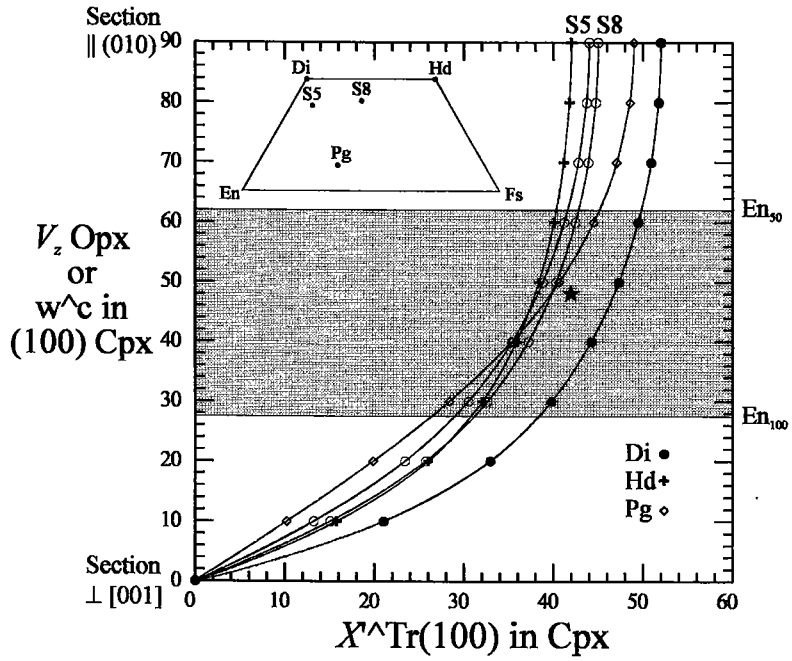

FIG. 7. Extinction angles for clinopyroxenes in epitactic overgrowth on orthopyroxene in sections cut normal to the common (100) plane. The shaded area delineates values that can be measured in sections cut normal to an optic axis of orthopyroxene. The star marks the location of a pair of values obtained on a grain from the 1881 lava flow. Inset shows the compositions of the pyroxenes for which the curves were drawn.

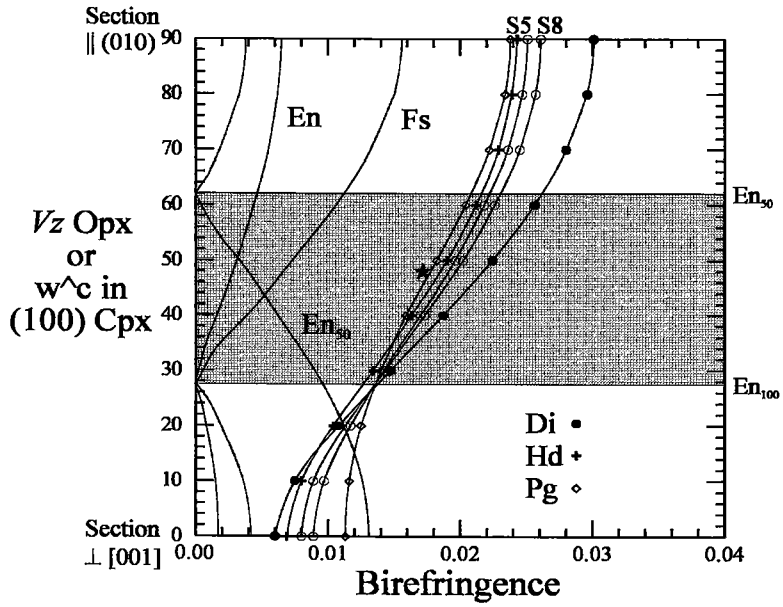

FIG. 8. Birefringence of clinopyroxenes in the zone normal to (100). See the caption of Figure 7 for an explanation of symbols.

Distinguishing epitactic overgrowths

If the overgrowths are epitactic rather than unoriented, it should be possible to predict the wave normal in the clinopyroxene given a wave normal in orthopyroxene. A wave normal that is easy to locate in the orthopyroxene is one parallel to an optic axis. The corresponding wave normal in clinopyroxene should then lie in (100) and at an angle to the common *c* axis equal to V_z for orthopyroxene. Consequently, curves can be constructed for optical properties *versus* the angle between the wave normal and the *c* axis for clinopyroxene crystals (Nicholls 1996). The measured optical property should fall on the appropriate curve for a clinopyroxene if the overgrowth is epitactic. If the different clinopyroxenes possess sufficiently contrasting optical properties, then epitactic overgrowths can be distinguished with the petrographic microscope. The properties that are easily determined in thin section are extinction angles, birefringence, and differences in indices of refraction between two phases (relief). The essence of the problem is to distinguish clinopyroxenes with low Ca-contents from those with high Ca-contents. If the clinopyroxene has a sufficiently low Ca-content, then the optic axial plane is normal to (010), whereas clinopyroxene with high Ca-contents have their optic axial plane parallel to (010).

Extinction angles for wave normals in (100)

Curves representing extinction angles between the fast direction and the trace of (100) for clinopyroxene overgrowths are shown in Figure 7. If the host orthopyroxene displays a centered optic axis, then the location of the wave normal is fixed (value on the *Y* axis) because, for a given orthopyroxene composition, V_z is determined (Deer *et al.* 1978; Table 3). If the wave normal in the clinopyroxene is parallel to an optic axis of the orthopyroxene, then the point for the extinction angle must fall in the shaded area on Figure 7. Over at least one-half the range of wave normals parallel to (100), the curve for pigeonite falls within the range of curves for augite (Fig. 7). Errors in the measurement of extinctions angles can occur for several reasons. For example, sections may not be exactly normal to (100), or the exact extinction position may be difficult to determine because of differences in composition or degree of order. Such problems make it difficult to distinguish pigeonite from augite in epitactic overgrowths with extinction angles.

Birefringence in sections normal to (100)

Curves representing the birefingence of epitactic pyroxenes in sections cut normal to (100) are shown on Figure 8. There is not a sufficient difference in birefringence

TABLE 6. RESULTS OF ELECTRON-MICROPROBE ANALYSES OF OLIVINE AS MICROPHENOCRYSTS AND IN THE GROUNDMASS

	c1	m1	r1	c2	m2	r2	c3	m3	r3
SiO_2	39.35	39.66	38.93	39.07	38.53	38.44	39.70	39.84	39.68
FeO	17.91	18.53	19.42	17.41	17.85	19.31	18.08	18.27	19.97
MnO	0.23	0.27	0.26	0.24	0.24	0.25	0.22	0.25	0.29
MgO	42.78	41.92	41.61	43.25	42.94	41.80	42.66	42.37	41.02
CaO	0.25	0.26	0.27	0.25	0.24	0.26	0.26	0.26	0.29
Total	100.52	100.64	100.49	100.22	99.80	100.06	100.92	100.99	101.25
				Mole Percent End Members					
Fo	80.51	79.61	78.74	81.09	80.62	78.92	80.31	80.02	77.99
Fa	18.91	19.74	20.62	18.32	18.80	20.46	19.10	19.36	21.30
La	0.34	0.35	0.37	0.34	0.32	0.35	0.35	0.35	0.40
Tp	0.25	0.29	0.28	0.26	0.26	0.27	0.24	0.27	0.31

	gm	gm	gm	gm	gm
SiO_2	38.52	39.24	39.03	39.21	40.03
FeO	19.28	19.06	23.73	19.58	19.55
MnO	0.26	0.27	0.27	0.28	0.25
MgO	41.24	41.81	37.46	40.58	41.33
CaO	0.28	0.27	0.34	0.29	0.29
Total	99.58	100.65	100.83	99.94	101.45
			Mole Percent End Members		
Fo	78.69	79.11	73.20	78.14	78.50
Fa	20.64	20.23	26.02	21.15	20.83
La	0.38	0.37	0.48	0.40	0.40
Tp	0.28	0.29	0.30	0.31	0.27

The proportion of oxides is expressed in wt.%.

between the clinopyroxenes to ensure a positive identification of the epitactic overgrowths in sections normal to (100). As a generalization, however, except in sections at a high angle to the *c* axis (section normal to [001]), clinopyroxenes with their optic axial plane (OAP) normal to (010) have a lower birefringence than Ca-rich pyroxenes.

Relief in sections normal to (100)

Figure 9 shows the relief expected between orthopyroxene (En_{85}, Fig. 3) and clinopyroxenes with compositions similar to those in the 1881 lava flow. The difference in relief should be low (0.02) between orthopyroxene and Ca-poor clinopyroxene, or moderate (0.04) between orthopyroxene and Ca-rich clinopyroxene, if the phases have the compositions observed for the flow. The "low" and "moderate" designations are to some degree subjective, but follow the guidelines given by Nesse (1991). The clinopyroxene should have a higher index of refraction than orthopyroxene in sections cut normal to (100), oriented with the trace of (100) parallel to the lower polarizer.

Most (approximately 9 out of 10) epitactic overgrowths in the 1881 lava flow have low to zero relief against the orthopyroxene. Where the orthopyroxene shows only one cleavage, the birefringence of the overgrowth or intergrowth is low (0.015), suggesting an initial Ca-poor overgrowth.

Olivine

Results of electron-microprobe analyses of olivine are listed in Table 6 for several typical crystals. A table listing results of all 33 spot analyses is available from the Depository of Unpublished Data, CISTI, National Research Council of Canada, Ottawa, Ontario K1A 0S2. The olivine microphenocrysts are normally zoned, with a range in composition of Fo_{82} to Fo_{73}. Olivine occurs primarily as microphenocrysts, between 400 × 200 μm and 200 x 150 μm, and uncommonly in the groundmass. Microphenocrysts are commonly skeletal and enclose glass, microlites and fine-grained groundmass assemblages.

Plagioclase

Results of electron-microprobe analyses of plagioclase are listed in Table 7 for several typical crystals. Plagioclase is a groundmass phase in the lava flow from the 1881 eruption. The crystals commonly are sufficiently large for analysis of both core and rim. The compositions determined in the 69 spot analyses range from An_{70} to An_{52}. The plagioclase grains display normal zoning. A table listing results of all 69 spot analyses is available from the Depository of Unpublished Data, CISTI, National Research Council of Canada, Ottawa, Ontario K1A 0S2.

TABLE 7. RESULTS OF ELECTRON-MICROPROBE ANALYSES OF FELDSPAR IN THE GROUNDMASS

	c1	r1	c2	r2	c3	r3	c4	r4	c5	r5
SiO_2	52.69	56.39	53.02	53.57	52.06	52.86	53.14	52.50	51.80	52.44
Al_2O_3	28.73	26.98	29.03	28.38	30.06	29.35	29.59	29.39	29.03	28.62
FeO	1.26	1.34	0.84	0.93	0.82	0.96	0.76	0.74	0.76	0.96
MgO	0.35	0.25	0.31	0.26	0.25	0.28	0.28	0.29	0.26	0.27
CaO	13.15	10.96	13.62	13.06	14.46	13.55	14.04	14.08	13.93	13.42
Na_2O	3.90	5.20	3.64	4.12	3.32	3.84	3.52	3.53	3.55	3.92
K_2O	0.09	0.17	0.07	0.09	0.06	0.08	0.08	0.07	0.08	0.09
Total	100.17	101.29	100.53	100.41	101.03	100.92	101.41	100.60	99.41	99.72
					Mole Percent End Members					
An	64.73	53.28	67.13	63.33	70.40	65.80	68.47	68.51	68.12	65.08
Ab	34.74	45.74	32.46	36.15	29.25	33.74	31.06	31.08	31.41	34.40
Or	0.53	0.98	0.41	0.52	0.35	0.46	0.46	0.41	0.47	0.52

The proportion of oxides is expressed in wt.%. BaO is below the limit of detection, 0.07 wt.%.

Where the overgrowth has a distinct relief against the orthopyroxene, the birefringence is near 0.02, suggesting an initial Ca-rich overgrowth. All the intergrown clinopyroxenes have low relief and low birefringence. The low-relief overgrowths commonly have been overgrown by clinopyroxene with higher birefringence. The optical characters of the pyroxenes indicate that the sequence of crystallization was orthopyroxene, followed by Ca-poor clinopyroxene, then by Ca-rich clinopyroxene.

Spinel

The 1881 lava flow contains both ilmenite–hematite and magnetite–ulvöspinel solid solutions in the groundmass. The grains of Fe–Ti oxides are too small for an adequate analysis, but are large enough to identify from ratios of intensities measured with the electron microprobe. One small cluster of cubes of Cr-rich spinel was found in skeletal olivine. The cubes are approximately 5 μm across. The

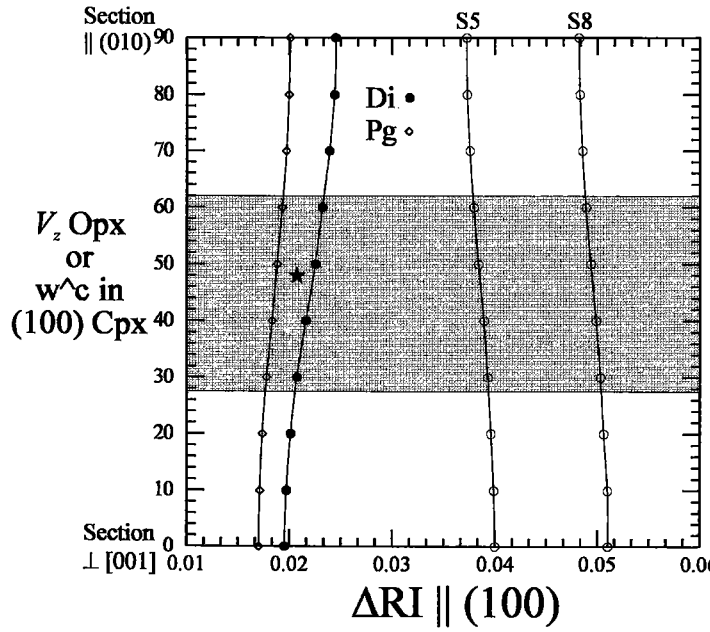

FIG. 9. Differences between the indices of refraction of orthopyroxene and clinopyroxene in the zone normal to (100) for thin sections oriented with the trace of (100) parallel to the lower polarizer, a measure of the relief of the clinopyroxene against the orthopyroxene. The clinopyroxene should have a higher index of refraction than the orthopyroxene. See the caption of Figure 7 for an explanation of symbols.

cluster may be a relic from an earlier stage of fractionation that gave rise to the 1881 flow. An average composition of the chromian spinel is listed in Table 8. The rock also contains an Fe-rich opaque mineral that lacks Ti, Mg, and Cr. It is most likely a sulfide (Table 1).

PATHS OF CRYSTALLIZATION

Paths of crystallization of melts calculated with the MELTS package (Ghiorso & Sack 1995) reproduce the mineral compositions found in the 1881 lava flow. The melt composition was modeled from the rock composition provided by Macdonald & Katsura (1964; Table 1). Predicted and observed compositions of the pyroxenes are compared in Figures 3B, C, and D. The crystallization sequence, required by the epitactic relationship, is

TABLE 8. AVERAGE RESULT OF ELECTRON-MICROPROBE ANALYSIS OF SPINEL

SiO_2 wt.%	0.08	FeO	23.72
TiO_2	2.34	MnO	0.34
Al_2O_3	14.17	MgO	8.01
Cr_2O_3	38.69	CaO	0.02
Fe_2O_3	12.65	Total	100.02

The proportion of Fe_2O_3 and FeO was calculated assuming stoichiometry.

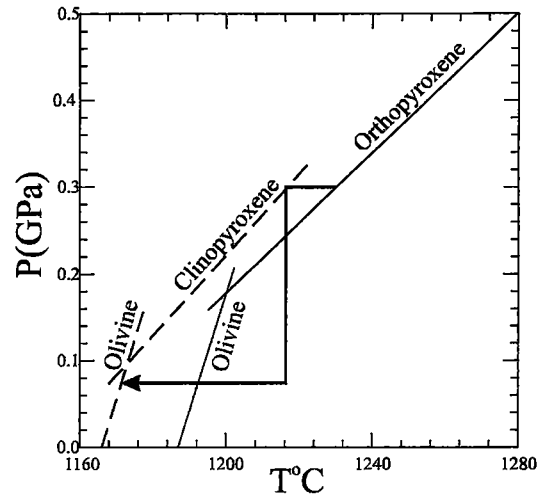

FIG. 10. Calculated liquidus (solid line) and first appearance curves (dashed lines) for conditions of fractional crystallization of a melt with the composition of the rock. Curves calculated with the thermodynamic data compiled by Ghiorso & Sack (1995). Calculations are for fugacity of oxygen values constrained by the ferrous-ferric ratio in the initial composition of the melt. Heavy curve with arrow is a possible path that will reproduce the phases found in the lava flow.

orthopyroxene, followed by pigeonite, then augite. The skeletal nature of the olivine is consistent with crystallization under conditions of rapid cooling. Presumably, these conditions would obtain at lower pressures, near or on the surface. Consequently, olivine likely reached saturation after the crystallization of the orthopyroxene phenocrysts.

Calculated liquidus and first-appearance curves under conditions of perfect fractional crystallization are shown on Figure 10. At pressures greater than 0.18 GPa, melts with the composition of the rock never saturate with olivine. At pressures greater than 0.18 GPa, 0.3 GPa for example, the sequence of pyroxenes found in the epitactic overgrowths is developed. If, after reaching clinopyroxene saturation, the magma is transported to shallower depths where pressures are less than approximately 0.1 GPa, olivine would be expected to crystallize. According to the MELTS model, the olivine would shortly cease to crystallize, and pigeonite and augite would then crystallize together (Fig. 3D).

The olivine composition predicted by the MELTS model at oxygen fugacities imposed by the Fe^{2+}–Fe^{3+} concentrations of the rock, assuming a closed system, is Fo_{80} (Fig. 3D). The most Mg-rich olivine analyzed is Fo_{82}, a value close to but significantly different from the predicted value. The 1σ analytical uncertainty is approximately $Fo_{0.08}$. At low pressures, plagioclase follows Ca-rich pyroxene in the fractionation sequence. Thermodynamic modeling predicts the initial plagioclase composition to be An_{73}. The most calcic measured composition is An_{70}, and the 1σ analytical uncertainty is $An_{0.04}$. The predicted and observed compositions are close, and the observed and predicted sequences of crystallization are the same.

Discussion

Relief of the overgrowths and intergrowths of clinopyroxenes against orthopyroxene can be used to indicate the chemical characteristics of the overgrowths and intergrowths. Ca-poor clinopyroxene has a lower relief against orthopyroxene than does Ca-rich clinopyroxene, at least in the 1881 lava flow. The chemical characteristics of the clinopyroxenes is consistent with the differences in birefringence between Ca-poor and Ca-rich pyroxenes. The epitactic relationships of orthopyroxene, Ca-poor pyroxene, and Ca-rich pyroxene are consistent with a stage of crystallization at a pressure greater than approximately 0.2 GPa. In order for the melt to saturate with olivine followed by Ca-poor pyroxene, a second stage of crystallization is required at pressures less than 0.1 GPa.

The classic view of a reaction relationship between olivine and Ca-poor pyroxene (Bowen & Anderson 1914) holds only at low pressure in the absence of significant amounts of dissolved H_2O (Kushiro *et al.* 1968; see Bloss 1994, p. 315). At pressures greater than approximately 0.3 GPa (Bloss 1994), $Mg_2Si_2O_6$ melts congruently, and the reaction relationship does not exist. In the 1881 flow, the analogous pressure is approximately 0.2 GPa (Fig. 10). At low pressures, olivine ceases to crystallize in the thermodynamic models of the 1881 lava flow when Ca-poor clinopyroxene reaches saturation. In high-pressure models, above 0.2 GPa, orthopyroxene and Ca-poor clinopyroxene crystallize together over a narrow range of temperature (5–15°C) before orthopyroxene ceases to crystallize.

Acknowledgements

The Natural Sciences and Engineering Research Council of Canada (NSERC) supported this work through research grant A7372. This manuscript benefitted from an internal review by E.D. Ghent and from reviews by A. Fowler, T.H. Pearce, and G.T. Nixon. A computer program, OPTICS, that calculates consistent optical properties and extinction angles for a variety of wave normals, is available through the World Wide Web at: http://www.geo.ucalgary.ca/~nicholls/optics.html.

References

Basaltic Volcanism Study Project (1981): *Basaltic Volcanism on the Terrestrial Planets*. Pergamon Press, New York, N.Y.

Bloss, F.D. (1961): *An Introduction to the Methods of Optical Crystallography*. Holt, Rinehart and Winston, New York, N.Y.

_____ (1994): *Crystallography and Crystal Chemistry*. Mineralogical Society of America, Washington, D.C.

Bowen, N.L. & Andersen, O. (1914): The binary system MgO–SiO_2. *Am. J. Sci.* **187**, 487-500.

Burden, R.L., Faires, J.D. & Reynolds, A.C. (1981): *Numerical Analysis*. Prindle, Weber & Schmidt, Boston, Massachusetts.

Deer, W.A., Howie, R.A. & Zussman, J. (1978): *Rock Forming Minerals. Single-Chain Silicates*. John Wiley & Sons, New York, N.Y.

_____, _____ & _____ (1992): *An Introduction to the Rock-Forming Minerals* (second ed.). Longman Group UK Limited, Essex, U.K.

Ghiorso, M.S. & Sack, R.O. (1995): Chemical mass transfer in magmatic processes. IV. A revised and internally consistent thermodynamic model for the interpolation and extrapolation of liquid–solid equilibria in magmatic systems at elevated temperatures and pressures. *Contrib. Mineral. Petrol.* **119**, 197-212.

Hess, H.H. (1960): Stillwater igneous complex, Montana. *Geol. Soc. Am., Mem.* **80**.

Kaplan, W. (1973): *Advanced Calculus*. Addison-Wesley Publishing Company, Reading, Massachusetts.

Kushiro, I., Yoder, H.S., Jr. & Nishikawa, M. (1968): Effect of water on the melting of enstatite. *Geol. Soc. Am. Bull.* **79**, 1685-1692.

LAUDER, W.R. (1961): Reaction of crystal structures and reaction fabric. *Am. Mineral.* **46**, 1317-1328.

LOCKWOOD, J.P. & LIPMAN, P.W. (1987): Holocene eruptive history of Mauna Loa Volcano. *In* Volcanism in Hawaii (R.W. Decker, T.L. Wright & P.H. Stauffer, eds.). *U.S. Geol. Surv., Prof. Pap.* **1350**, 509-535.

MACDONALD, G.A. & KATSURA, T. (1964): Chemical composition of Hawaiian lavas. *J. Petrol.* **5**, 82-133.

MARSDEN, J.E. & TROMBA, A.J. (1981): *Vector Calculus*. W.H. Freeman and Company, San Francisco, California.

MORIMOTO, N. (1989): Nomenclature of pyroxenes. *Can. Mineral.* **27**, 143-156.

NESSE, W.D. (1991): *Introduction to Optical Mineralogy*. Oxford University Press, New York, N.Y.

NICHOLLS, J. (1996): Location of ray paths for a known wave normal in biaxial crystals. *Can. Mineral.* **34**, 161-170.

_____. & STOUT, M.Z. (1986): Electron-beam analytical instruments and the determination of modes, spatial variations of minerals and textural features of rocks in polished section. *Contrib. Mineral. Petrol.* **94**, 395-404.

PHILLIPS, W.R. & GRIFFEN, D.T. (1981): *Optical Mineralogy, The Nonopaque Minerals*. W.H. Freeman and Company, San Francisco, California.

PRESS, W.H., TEUKOLSKY, S.A., VETTERLING, W.T. & FLANNERY, B.P. (1992): *Numerical Recipes in FORTRAN, The Art of Scientific Computing* (2nd ed.). Cambridge University Press, Cambridge, U.K.

TARNEY, J. (1969): Epitaxic relations between coexisting pyroxenes. *Mineral. Mag.* **37**, 115-122.

THOMAS, G.B., JR. (1968): *Calculus and Analytic Geometry* (fourth ed.). Addison-Wesley Publishing Co., Reading, Massachusetts.

THOMPSON, J.B., JR. (1982): Composition space: an algebraic and geometric approach. *In* Characterization of Metamorphism through Mineral Equilibria (J.M. Ferry, ed.). *Rev. Mineral.* **10**, 1-32.

WRIGHT, F.E. (1951): Computation of the optic axial angle from the three principal refractive indices. *Am. Mineral.* **36**, 543-556.

Received October 2, 1996, revised manuscript accepted June 25, 1997.